# **ORGANOMETALLICS**

pubs.acs.org/Organometallics Tutorial

# Elemental Aspects of Transition Metals Pertinent to Organometallic Chemistry: Properties, Periodicity, Curiosities, and Related Main Group Issues

Peter T. Wolczanski\*

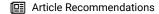


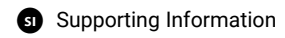
Cite This: Organometallics 2024, 43, 787-801



**ACCESS** I

Metrics & More





**ABSTRACT:** This tutorial on transition metal chemistry—sans the lanthanides and actinides—is intended as preliminary information for a high-level undergraduate (UG) inorganic, organometallics, or a comparable first-year graduate (G) course. It features ionization energies (IEs) and comparative nd and (n+1)s orbital energies, electron affinities (EAs), electronegativities (ENs), and covalent radii  $(c_r)$ . Redox properties of

 $\begin{array}{lll} \textbf{TM} = \text{transition metal} \\ \hline E^{\circ} \ (M^{+} \sim M)^{\parallel} & E^{\circ} \ \ c_{TM} \\ \hline (M^{2^{+}} \sim M) & EA \ \ \textbf{TM} \\ \hline (M^{3^{+}} \sim M)^{*} & EA \ \ \textbf{TM} \\ \hline (M^{4^{+}} \sim M)^{\ddagger} & EA \ \ \textbf{E} \\ \hline (MO_{\chi}^{n^{+}} \sim M)^{\$} & EA \ \ \textbf{E} \\ \hline \end{array}$ 

appropriate aquo complexes ( $\Delta E^{\circ}_{red} = E^{\circ}(red)$ ) are also included due to their impact on critical properties and reactivity, as are pertinent aspects of the main group elements.

## INTRODUCTION

Many in the organometallic community teach aspects of the periodic table in freshman and initial inorganic offerings, and while the categorizing of elements is profound, rationalizing their properties can be challenging. Specifically, while aspects of alkali, alkaline earth, and p-plock elements can be safely explained with electron configurations, concepts like Z<sub>eff</sub>, and periodicity, properties of the transition metals (TMs), lanthanides, and actinides are often misinterpreted. In many instances, freshman textbooks eliminate the TM core of the periodic table in an anti-Mendeleevian purge, ultimately causing confusion when certain trends in main group (MG) elements are erroneously assumed to translate to the transition metals. In consideration, and with some trepidation, a closer inspection of the nd (n = 3-5) metals (the lanthanides and actinides are hereby left for those more qualified), appears warranted, given their modest treatment by the writers of freshman textbooks.

When teaching the first course involving TMs at either the UG or G level—either an inorganic<sup>2</sup> or organometallics course<sup>3,4</sup>—an initial foray into the periodic table provides an introduction. In-depth information is often limited to the MG, and this treatise is an effort to provide the equivalent background information on TMs, in addition to the general descriptions that are typical (early or late, high- or low-valent, high- or lowcoordinate, common oxidation states, etc.). Curiosities have also cropped up during educational and research endeavors. For example, many of the specific aspects discussed below reflect personal experiences in reviewing manuscripts, etc., where the misinterpretation of TM properties was of concern. As a consequence, this essay/tutorial is an entreaty for the community to use and assess periodicity to a deeper extent with regard to TM atomic properties, and the rationalization of corresponding coordination chemistry. It is written as introductory material for an undergraduate inorganic or firstyear graduate inorganic/organometallic course; more rigorous, focused information can be found in the primary literature. None of the interpretations are original, stemming simply from the principles taught in freshman and undergraduate inorganic chemistry, and most of the data is freely available from NIST (https://www.nist.gov/chemistry). In addition, the author welcomes all correspondence concerning all topics, peccadillos, and peculiarities.

# ■ THE TUTORIAL

**I. The Main Group.** Before tackling the TMs, a few comments regarding the MG elements are pertinent to complex formation, notably regarding the assessment of ligands. Relative ionization energies, electron affinities, atomic and ionic radii, etc., are the purview of freshman textbooks and will not be discussed. The chart in Figure 1 is a handy compilation of this data, with inclusion of covalent radius (Pauling) as a replacement of the aforementioned radii. <sup>5-9</sup> Reduction potentials of alkali, alkaline earth, and p<sup>1</sup> elements are included, but the remainder of the MG is difficult to assess due to speciation (the variation in the structure of aqueous complexes complicates analysis) and are left to the reader to research and peruse if curious.

*l.A. Reduction Potentials.* It is interesting that reduction potentials of the alkali metals  $(M^+ + e^- \rightarrow M)$  are roughly equivalent  $(\Delta E^{\circ}_{red} \text{ (ave)} = -2.94(13) \text{ V; } -F\Delta E^{\circ} \text{ (ave)} =$ 

Received: December 21, 2023 Revised: March 1, 2024 Accepted: March 4, 2024 Published: March 29, 2024





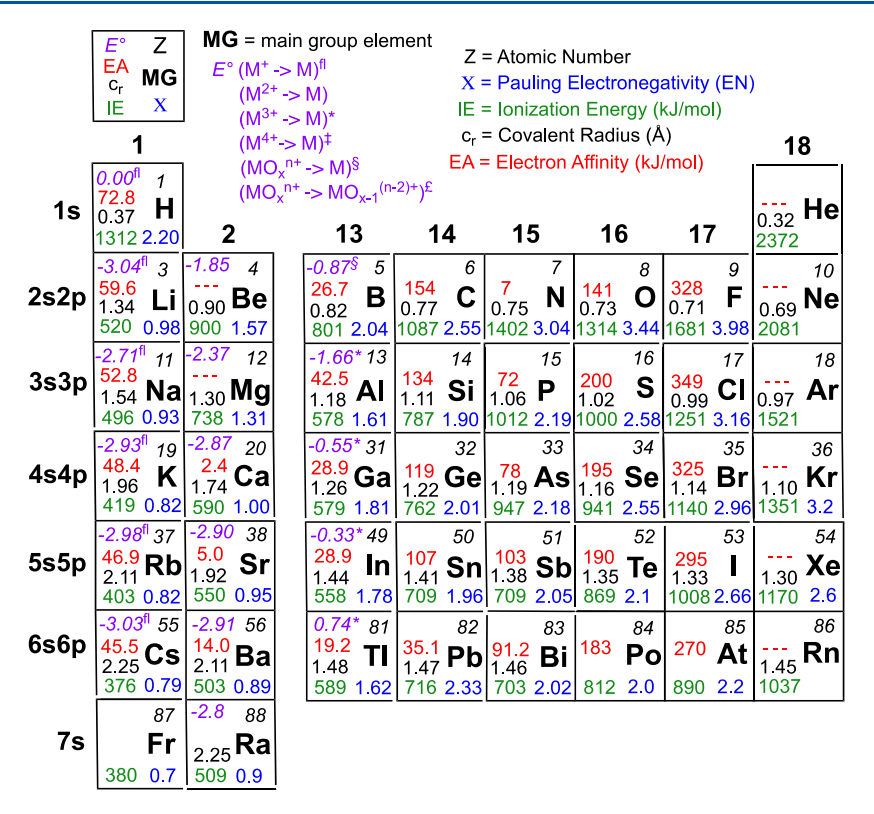


Figure 1. Main group elements with pertinent data according to the key in the upper left.

283(13) kJ/mol), in stark contrast to corresponding ionization energies and heats of sublimation, as shown in Figure 2. Entropic factors are not included (more sophisticated treatments are available), <sup>10</sup> since the gist of the reduction factors are

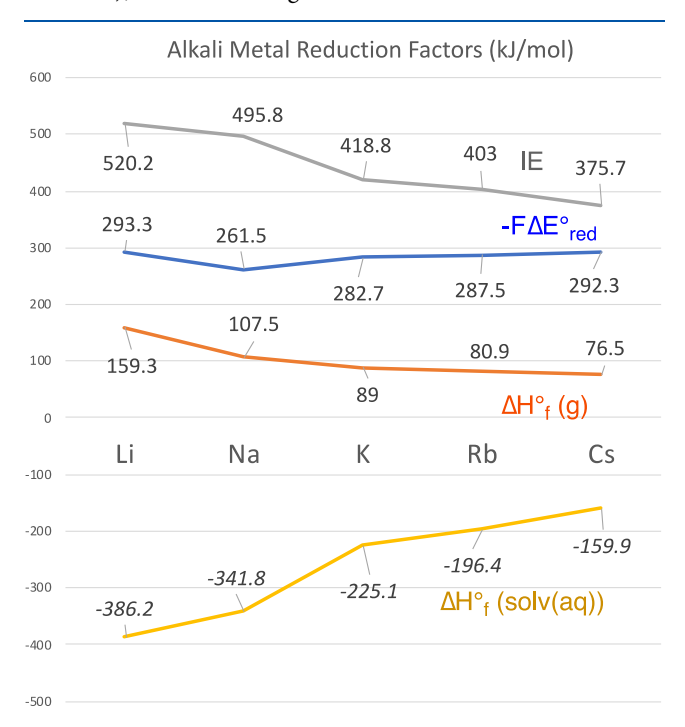


Figure 2. Neglecting entropies, a rough enthalpy summation of contributions to  $\Delta E^{\circ}_{\rm red}$  (as  $-{\rm nF}\Delta E^{\circ}_{\rm red}$ , blue), is illustrated in this chart. Note that compensation for heats of sublimation ( $\Delta H^{\circ}_{\rm f}$  (g), orange) and ionization energies (IEs, gray) occurs in solvation energies,  $\Delta H^{\circ}_{\rm f}$  (solv(aq), gold):  $-{\rm F}\Delta E^{\circ}_{\rm red} = \Delta H^{\circ}_{\rm f}$  (g) + IE +  $\Delta H^{\circ}_{\rm f}$  (solv(aq)).

enthalpic. <sup>10</sup> Differences in aqueous solvation energies, which are significantly less favorable descending from  $\operatorname{Li}^+(OH_2)_n$  to  $\operatorname{Cs}^+(OH_2)_m$ , compensate for ionization energies (IEs) and heats of sublimation, and render the aqueous potentials remarkably similar. In common nonaqueous inorganic and organometallic chemistry, the medium of the reducing agent (e.g., the Hg in Na/Hg, the "C<sub>8</sub>" in KC<sub>8</sub>, etc.) has significant consequences besides mediating electron transfer and ease of use, because it allows the reduction potential to be manipulated.

The above breakdown of potential  $(\Delta G^\circ)$  to enthalpy requires the assumption that entropy differences are not critical (or cancel out), and there are other complications and perspectives for the remainder of the MG. The trend essentially follows for the alkaline earths, where the reduction potential refers to  $M^{2+} + 2e^- \to M$  in aqueous solution. In this case, the disproportionately high ionization energies and  $\Delta H^\circ_{\ \ f}(g)$  values for Be and, to some extent, Mg ( $(M \to M^+ + e^-) + (M^+ \to M^{2+} + e^-)$ ) are not as readily compensated by favorable solvation energies of the divalent ions, and the potentials reflect these factors. Once the p-block is accessed, reduction potentials are not easily interpreted, as speciation, multiple ionization energies, and orbital origins are consequential, hence they are not included in Figure 1, except for group 13.

included in Figure 1, except for group 13. Electronegativity  $(EN)^{5,11-18}$  is an extremely valuable concept in chemistry (the familiar Pauling X values are used) as a logical construct in partitioning charge in a chemical bond. Essentially defined as the ability of an atom or group of atoms to attract electrons toward itself within a bond, it serves as a basis for chemical intuition to the budding chemist. The higher the X value, the greater the attraction, and in MG applications, there is a general tendency from "low left" to "high right" values in the Periodic Table, with a few discrepancies that can be explained by the scandide contraction (vide infra). In group 13, there is a correlation with  $\Delta E^{\circ}_{\rm red}$  ( $M^{3+} + 3e^{-} \rightarrow M$ ), as

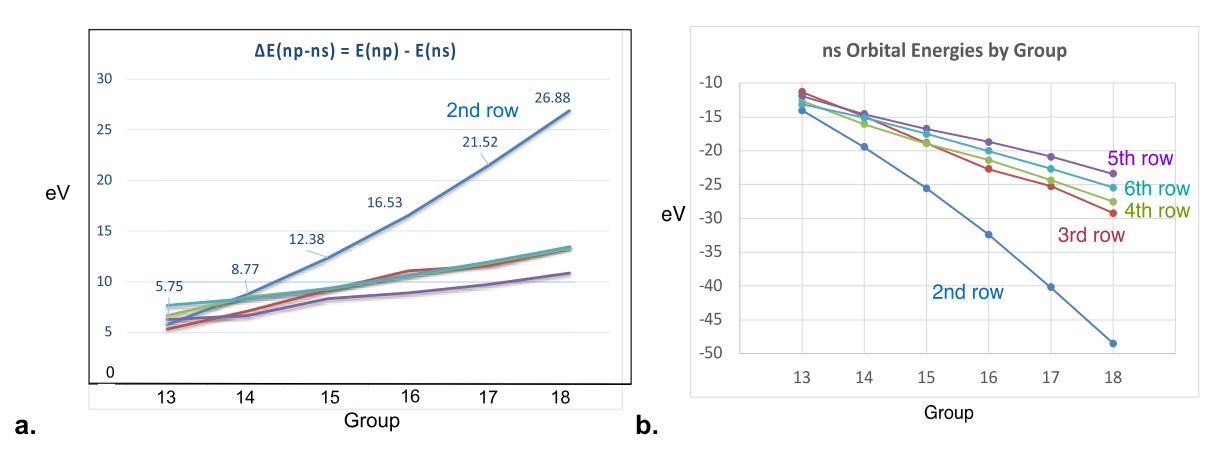


Figure 3. a. MG  $\Delta E_{\rm np-ns}$  for the groups 13–18 graphed by row (color coded as in b.). The energy gaps for the 3rd, 4th, 5th, and 6th MG rows are very similar; pertinent row ns, np, and  $\Delta E_{\rm np-ns}$  values from photoelectron spectroscopy (PES) are given in Supporting Information. b. The ns orbital energies by group.

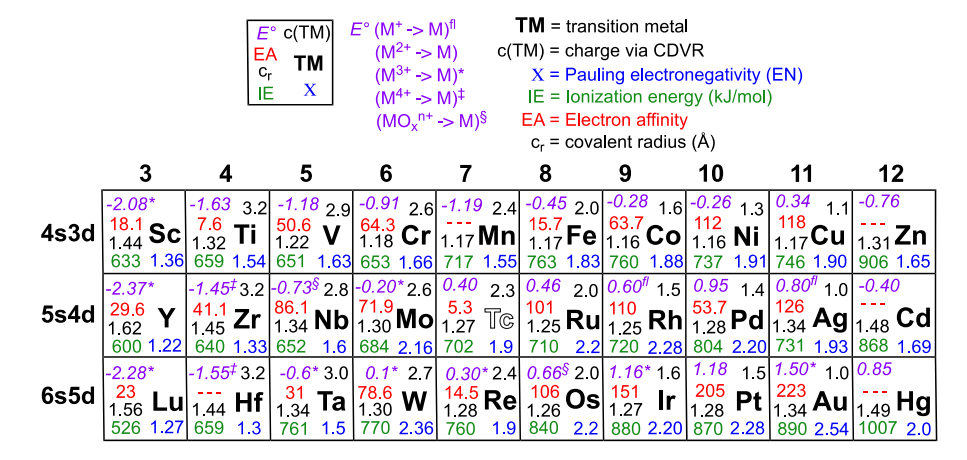


Figure 4. Transition metal elements, sans the lanthanides and actinides, with pertinent data according to the key in the upper left.

the change to  $Ga^{3+}$  and  $In^{3+}$  becomes less and less negative and the  $Tl^{3+}$  reduction potential turns positive (0.74 V). The EN generalization is an utter failure for the TMs, as will be elaborated later.

I.B. Hybridization. Hybridization in MG elements is often misconstrued, as a cursory examination of bond angles of the pnictogen hydrides ( $\angle$ HEH in EH<sub>3</sub>: E = N, 107.8°; P, 93.5°; As, 91,8°; Sb, 91.7°; Bi, 90.5°) and related geometric entities indicates minimal hybridization below the second row. In addition, studies on the inert pair effect reveal the minimal participation of ns orbitals in bonding, although there is still some discussion about their influence on chemical structure. Two factors are usually used to rationalize the absence of hybridization:  $\Delta E_{\rm np-ns} = E_{\rm p} - E_{\rm s}$ , and spatial diffusivity. In Figure 3a, the  $\Delta E_{\rm np-ns}$  (in eV) is plotted for each row, and it is obvious that the only row that shows a significantly increasing gap corresponds to n = 2, the only row that is thought to exhibit *hybridization.* The n = 2 data does show that  $\Delta E$  increases with atomic number, hence hybridization is attenuated as exemplified in commonly taught homodiatomic MO diagrams, in which 2s/ 2p mixing is consequential for Z = 5-7, and contributes minimally to dioxygen and difluorine. What is clear is that the  $\Delta E_{\rm np-ns}$  rationale for hybridization in general is completely incorrect.

Figure 3b also shows that the ns orbitals decrease in energy across a row, as screening effects diminish, but there is only a subtle increase in spread of the ns energies within a column for n

= 3–6. Interestingly, the trend is reversed for the fifth and sixth rows, as poor shielding from  $4f^{14}$  electrons impacts the order. Since Figure 3a shows that  $\Delta E_{\rm np-ns}$  does not hamper or prevent hybridization, its absence in rows 3 through 6 must be due to the spatial distribution of the ns and np (n > 2) orbitals. As n increases, the size of the corresponding s orbital increases substantially, its number of radial nodes (n - l - 1) increases, and the radial nodes of the related np orbital also increase. The consequences of greater size, and the distribution of radial nodes in the component orbitals, leads to negligible net overlap. This spatial diffusivity is the main factor for the dearth of hybridization for ns/np (n = 3–6) orbitals, and contributes to the inert pair effect.

The origin of hybridization in the second row MG elements lies in kainosymmetry, which refers to the first atomic orbitals of the angular momentum (azimuthal) quantum number, l, which have no radial nodes (i.e., 1s, 2p, 3d, 4f, etc.). <sup>19,20</sup> Also referred to as kainosymmetric, these orbitals poorly screen nuclear charge and are relatively contracted. Consequently, the radial extent of the 2p orbital is similar to the 2s, and hybridization is consequential despite differences in energy (Figure 3,  $\Delta E_{\rm 2p-2s}$ ) that attenuate the mixing as  $Z_{\rm eff}$  increases. With no radial nodes, the 2p orbital has the critical net overlap with the 2s, even though the latter has one radial node. Poor screening by the 3d<sup>10</sup> electrons is the origin of the scandide contraction, which impacts some properties of period 4, such as the anomalous IE of Ga (or, more significantly, the sum of IEs 1–3). The lanthanide

contraction is the most noteworthy of kainosymmetric effects, as poor screening by 4f<sup>14</sup> electrons causes the radii of the secondand third- row TMs to be quite similar, in addition to affecting properties of MG period 6.

I.C. Points of Emphasis. 1) The medium (solvent, ligand, etc.) in reducing agents, principally in organometallic applications, is important in mediating electron transfer and redox potential, hence aqueous potentials can sometimes be deceiving. 2) sp-Hybridization is observed only in the second row, where kainosymmetry—the absence of radial node(s) of the 2p orbital—permits it to mix with the 2s orbital until the energy gap between the two orbitals limits this interaction. 3) Main group rows 3–6 do not engage in hybridization even though the  $\Delta E_{\rm np-ns}$  values are not prohibitive. The lack of hybridization in rows 3–6 is a consequence of poor spatial overlap of the ns and np (n = 3–6) orbitals, principally due to their radial nodes.

II. Transition Metals. II.A. General. A compilation of the transition metals<sup>21</sup> and pertinent properties are illustrated in Figure 4 in the form of the d-block of the periodic table. A key is provided, and much of the data provided parallels the standard information given to freshman or included in other introductory courses. In the table, reduction potentials and a rough measure of the charge state of an element relative to Fe(2.0+) are included in addition to the typical assembly of ionization energies, electron affinities, electronegativity, and covalent radii. The charge state is courtesy of this laboratory's investigations into a benchtop means of assessing a single relative charge for each transition metal in lieu of listing oxidation states, termed Charge Distribution Via Reporters (CDVR).<sup>22</sup> If the reader is not familiar with this gedanken experiment, the values roughly correspond to an average of the formal oxidation states of each specific element. Note that some latitude in the assessment of TM properties is required, as Zn, Cd, and Hg are sometimes removed from consideration when they are clear outliers.<sup>23</sup>

II.B. Elemental Oxidation. II.B.1. General Ionization Energies. For main group species, particularly the p-block, screening factors for ns and np orbital electrons are used to coarsely explain ionization energies. The simple model assumes the electron being ionized from a coulomb potential (i.e.,  $-(Z_{eff})e/r$ , where  $Z_{eff} = Z + (shielding from the remaining)$ electrons)) is the effective nuclear charge. More sophisticated treatments involving angular momenta can be utilized, but a modest riff on the Bohr model needs only the principal quantum number (n) to afford the equation: IE (kJ/mol) =  $1312(Z_{\text{eff}}^2/$ n<sup>2</sup>). This largely suffices in explaining the general increase in IE that occurs across a row, as successive electrons screen less effectively (Z<sub>eff</sub> increases). Anomalies occur due to relief from Coulombic repulsion (e.g., IE(N) = 1402 kJ/mol, whereas IE(O) = 1314 kJ/mol), although these diminish down the table as  $r_{12}$  ( $r_{12}$  is the "average" distance between electron pairs) increases. As one descends the table in the s- and p-blocks, ionization energies diminish, because while Zeff is increasing, the principal quantum number n is increasing to a greater extent, thereby decreasing the  $(Z_{eff}/n)^2$  term.

Complications within the d-block largely limit the utility of these explanations from being applicable to TMs. <sup>24</sup> Application of the Bohr model to transition metals can explain the very general increase across each row of the periodic table, but the increases in IE are not as dramatic, as the first, second, and third rows have ranges of  $\sim$ 273,  $\sim$ 268, and  $\sim$ 484 kJ/mol, respectively, as shown in Figure 5. The increase in IE across a row is also relatively smooth in the progression from the early metals to the

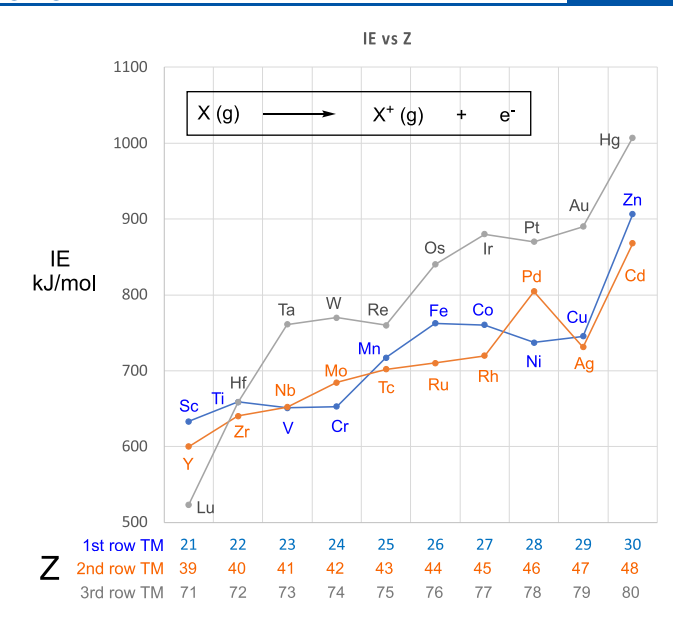
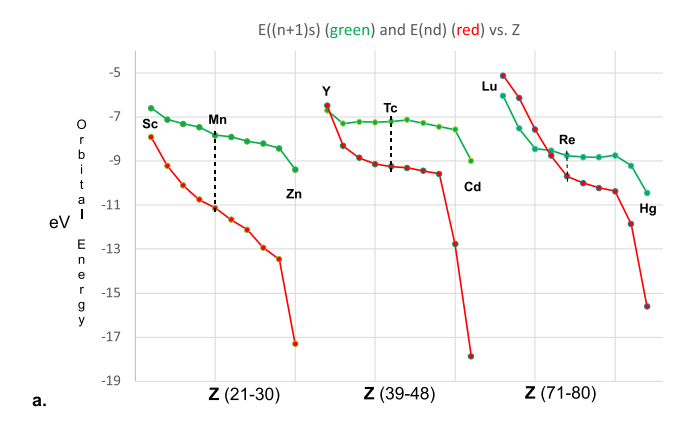


**Figure 5.** Gas phase ionization energies (IEs) of the transition metals in kJ/mol.

late, as nd shielding diminishes. Unlike the MG, the variation descending the table does not follow the aforementioned  $(Z_{\rm eff}/n)^2$  logic, as the first- and second-row transition elements are very similar, averaging 722 and 711 kJ/mol, respectively, with the third-row series substantially higher, averaging 796 kJ/mol. For the first and second rows,  $(Z_{\rm eff}/n)^2$  averages  $\sim\!0.54$ , while the third row averages  $\sim\!0.60$ . Keeping explanations within the Bohr model, poor screening by the kainosymmetric 3d orbital electrons renders second-row IEs higher than expected. Subsequent ineffective screening by the kainosymmetric  $4f^{14}$  electrons, i.e., the lanthanide contraction,  $^{25}$  some modest relativistic effects,  $^{26}$  and additional inefficient screening by 5d electrons all contribute to the remarkable increase in the third ionization energies.

II.B.2. Orbital Energies. Figure 6 illustrates the respective (n +1)s and nd orbital energies for the three rows (6a), and the  $\Delta E = E(nd) - E((n+1)s)$  (6b), as determined from photoelectron spectroscopy (PES).<sup>27</sup> The PES orbital energies reflect the instantaneous ejection of an electron from TM (g), the vertical ionization energy, and are taken as an indication of the orbital energy from which it derives. The corresponding adiabatic ionization energy is one means of determining the IE, which is essentially the thermodynamic energy difference between neutral TM (g) and TM<sup>+</sup> (g).

From just an orbital energy standpoint, the numbers belie the filling chart paradigm practiced in freshman chemistry, and  $e^2/r_{12}$  factors, etc., must be recognized to reconcile many IEs and pertinent electron configurations. W. H. E. Schwartz<sup>28,29</sup> has delineated five factors needed to understand electron configurations: 1) d-orbital collapse; 2) nd vs (n+1)s electron repulsions; 3) (n+1)s Rydberg destabilization; 4) configurations and states; and 5) relativistic spin—orbit coupling. Rydberg destabilization rationalizes why TM complexes (i.e.,  $L_m X_o M^p$ ) may be simply described as nd², as perturbation of the diffuse (n+1)s orbitals by the ligands raises their energy well above the nd. Relativistic and spin—orbit effects can be on the order of hundreds of kJ/mol for high Z, and impact ground state (GS) configurations and states, but require advanced knowledge and will be generalized if necessary.



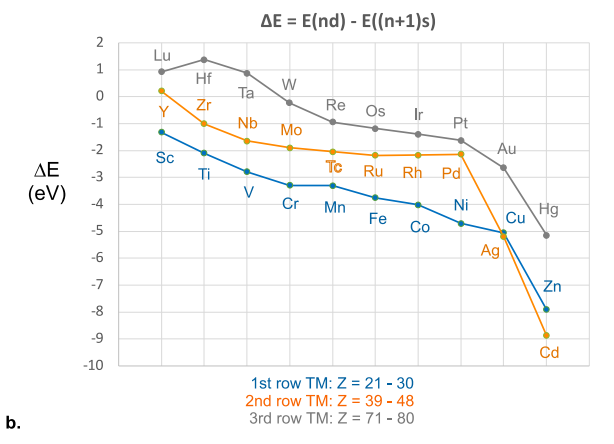


**Figure 6.** a. Energies for (n+1)s and nd orbitals vs Z (1st, 2nd, and 3rd rows) taken from PES data. b.  $\Delta E(nd - (n+1)s)$  vs Z for the TMs.

Orbital energies obtained by PES reveal the orbital sequence from Ca ([Ar]4s²) where 3p  $\ll$  4s < 3d changes at Sc ([Ar]3d¹4s²) and subsequent TMs, where 3p  $\ll$  3d < 4s. Note that Y in the second row, and Lu, Hf, and Ta in the third row are the few exceptions where (n+1)s > nd in energy. It is important to note the gap ( $\Delta E$ ) between (n+1)s and nd orbital energies closes as the periodic table is descended, as aspects of (n+1)s/nd

orbital mixing apparent in coordination and organometallic chemistry are elemental in origin. Not only does  $\Delta E$  get smaller, but oddities exist. As Figure 6b illustrates, the energy gap is remarkably flat for Nb–Pd, as are the 5s and 4d orbital energies, allowing for greater variation in electron configurations. The trends roughly parallel those of the ionization energy (i.e., IE roughly correlates with  $-E(highest\ orb)$ ), which generally occurs from the (n+1)s orbital, but there is considerable variation.

II.B.3. Pairwise Interaction Approach. In instructing inorganic/organometallics students at the UG/G (1st yr) level, an elementary look at interelectron energies should suffice in rationalizing, or at least revealing, the complication in assessing electron configurations critical to IEs. Figure 7 shows a basic approach, where the operator  $e^2/r_{12}$  assesses pairwise interactions in the orbital portion of the wave function over an "average" distance between electron(1) and electron(2)  $(r_{12})$ . The examples feature two electrons in one or two orbitals, but the pairwise exchange premise can be extended to multiple orbitals. Since an electron wave function is antisymmetric, either its orbital function or its spin function must be antisymmetric (must change signs upon swapping electrons), but not both. This approach can be used to estimate energy differences in GS and excited state (ES) configurations (ignoring interorbital coulomb, exchange terms; estimate  $K \sim C \sim 2C'$  in magnitude) for certain elements that differ from placement of a single electron (e.g., Cr(GS) [Kr]5s<sup>1</sup>4d<sup>5</sup> and Cr(ES) [Kr]5s<sup>2</sup>4d<sup>4</sup>, etc.).

Most familiar is the coulomb energy, C, that arises from the occupation of one orbital with two electrons (case 1), which is symmetric, mandating an asymmetric spin function. For example, double occupation of an ns orbital features this repulsion energy, C(ns). Less familiar are the factors derived from orbital wave functions in which electrons occupy two different orbitals of the same type (cases 2 and 3). Application of the repulsion operator to an orbital function of this type leads to an energy expression with three integrals, two of which are different. Two of the integrals are Coulombic and represent interorbital repulsions common to both cases (C'), and the second type of integral is an exchange type. If the two electrons in two different orbitals are symmetric with respect to exchange,

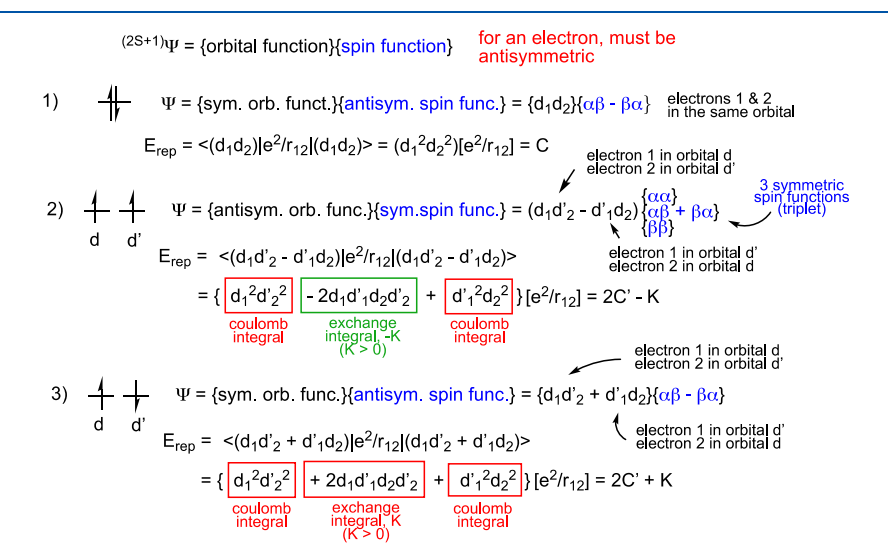


**Figure 7.** Basic, two-electron unnormalized wave functions used to delineate the types of interelectron repulsions that factor into state energies pertaining to electron configurations. Three types of symmetric spin functions (S = 1, 2S + 1 = 3 (triplet)) are associated with antisymmetric orbital functions (2), while one antisymmetric spin function is affiliated with symmetric orbital functions (1 and 3).

i.e., they have the same  $m_s$  values and possess a symmetric spin function, then the exchange integral -K (K>0, a positive integral) represents a *stabilization* (case 2). If the spin function changes sign as the electrons are swapped (exchanged), it is antisymmetric, and the corresponding orbital function is symmetric, with an exchange integral +K that indicates a *destabilization*. The ground state configurations of the neutral and cationic ( $Z^+$ ) elements can be assessed in terms of E(ns), E(nd), C, C', and  $\pm K$ , keeping in mind that the actual  $r_{12}$  changes among different orbitals, different numbers of electrons, and, *significantly in ions vs neutral atoms* (Figure 8). Note that

3d <sup>n</sup> configuration	E(3d <sup>n</sup> )	#C	#(2C' - K)	#(2C' + K)	E'(tot)
4	1	0	0	0	E(3d)
+ +	2	0	1	0	2E(3d)-K+2C'
+ + +	3	0	3	0	3E(3d)-3K+6C'
+ + + + -	4	0	6	0	4E(3d)-6K+12C'
4 4 4 4 4	5	0	10	0	5E(3d)-10K+20C'
# + + + +	6	1	10	4	6E(3d)+C-6K+28C'
# # 4 4 4	7	2	11	8	7E(3d)+2C-3K+38C'
# # # + + +	8	3	13	12	8E(3d)+3C-K+50C'
# # # # +	9	4	16	16	9E(3d)+4C+64C'
<del>                                    </del>	10	5	20	20	10E(3d)+5C+80C'

**Figure 8.** Contributions to total energy E'(tot) from  $1e^-(E(3d^n))$  and  $2e^-(C, 2C - K, 2C + K)$  integrals in  $3d^n$  configurations from Figure 7.

orbital energies are derived from 1e<sup>-</sup> operators assessing kinetic energy and nuclear attraction, whereas the remaining 2e<sup>-</sup> integrals are factors of interelectron repulsion. Beyond the scope of this treatment are effects from angular momenta, spin—orbit, relativistic factors, etc.

II.B.4. First-Row TM IEs. Figure 9 shows a good correlation with -E(4s) (relative to the ionized electron at 0.0 eV), which increases in energy across a row (E(4s) decreases) obtained from PES data. All the ionizations occur from the 4s orbital in the Ti–Zn series, and the red connectivity implicates a smooth increase, as screening factors diminish. Deviations of IE are due to the various interelectronic components discussed above as

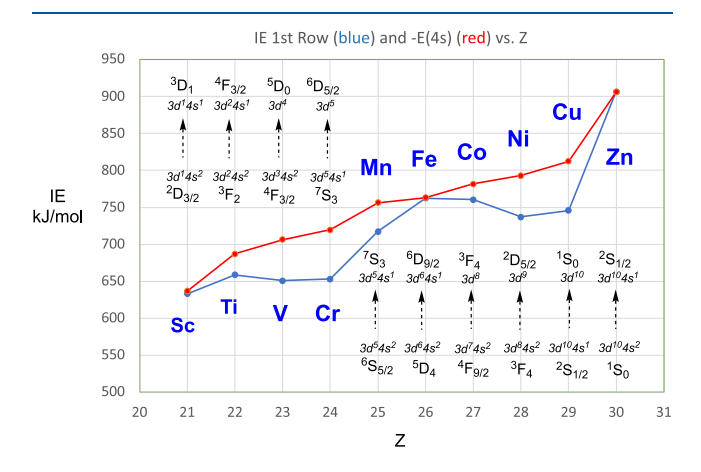


**Figure 9.** Plots of IE (blue, kJ/mol) and -E(4s) orbital (red, kJ/mol) from PES for the first row of the transition elements. Electron configurations and states (NIST) are given for the  $M^0$  (g) (below) and  $M^+$  (g) (above).

applied to both a neutral atom and its cation with a smaller  $r_{12}$  that renders interelectron Coulombic (C, C') and exchange ( $\pm K$ ) factors larger.

The first significant deviation in Figure 9 occurs for V, where ionization occurs with a change from <sup>4</sup>F<sub>3/2</sub>, with its 3d<sup>3</sup>4s<sup>2</sup> configuration, to the cation  ${}^5D_0$ , with its  $3d^4$  configuration. This is a great example of the complications in TM IEs, as the ionization involves numerous factors: 1) a relief from C(4s) repulsion; 2) a change from 4s to 3d occupation, presumably due in part to E(3d) < E(4s); 3) an increase in favorable exchange energy which also reflects K(cation) > K(neutral); 4) an unfavorable change in number (6 more) and magnitude of interelectronic repulsions C' (C'(cation) > C'(neutral)). Schwartz chooses to evaluate this in reverse. "Because the 3d shell is rather compact, in contrast to the diffuse Rydberg 4s orbital, the electron repulsion in the d shell increases strongly with increasing d occupation. Eventually, it becomes energetically favorable to shift one or even two electrons from the 3d shell into the slightly higher energy 4s, where the electronic Coulomb repulsion is much smaller. A remarkable example is V<sup>+</sup>  $(3d^4) + e^- \rightarrow V^0 (3d^34s^2)$ . Similar situations are well-known in ligand-field theory for low-spin versus high-spin transition-metal complexes."28 These same factors are responsible for the GS of Cr being  $3d^54s^1$  ( $^7S_3$ ), which undergoes a relatively simple ionization from 4s.

The remaining IEs occur via loss of a 4s electron, but once the 3d orbitals are half-filled, the  $\Delta E(3d-4s)$ , which is increasingly negative, cannot compensate for an additional C(3d), hence for Mn and Co, an electron stays in 4s. After Co,  $\Delta E(3d-4s)$  is great enough to compensate for the increasing C'(3d) factors, as  $r_{12}$  does not change substantively for the neutral atoms or the cations since repulsions from additional electrons compensate for diminished screening.

II.B.5. Second-Row TM IEs. Figure 10 illustrates the second-row IEs (orange) that gradually increase as electron screening

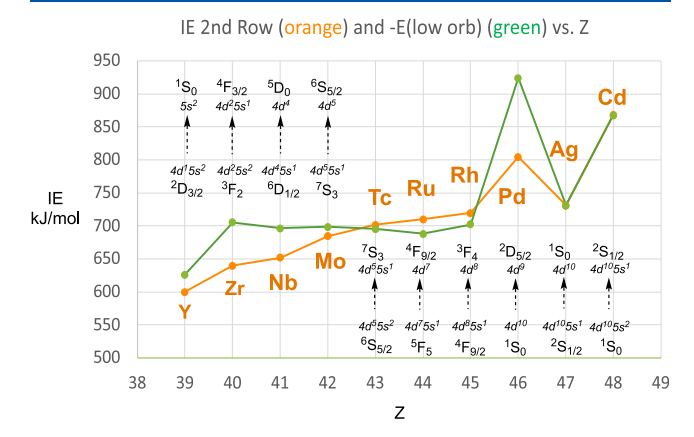


**Figure 10.** Plots of IE (orange, kJ/mol) and -E of the low valence orbital (green, kJ/mol) from PES for the second row of the transition elements. Electron configurations and states (NIST) are given for the  $M^0$  (g) (below) and  $M^+$  (g) (above).

becomes less effective, and -E(low orbital, green) energies from PES that are remarkably flat from Zr to Rh corresponding to ionization from Ss. Release of coulomb energy for Zr renders its IE less than predicted by PES, but ionization occurs from the Ss<sup>1</sup> neutral GS of Nb, and still the IE is 50 kJ/mol lower than that predicted by PES. Apparently more favorable exchange energies (6(-K + 2C')) for  $4d^4$  in both neutral and cation) in the cation due to  $r_{12}$  changes cause the IE to be lower than -E(5s). These

factors attenuate for Mo (-10(K + 2C')) for 4d<sup>5</sup> in both neutral atom and cation). At Tc, as Zeff continues to increase, core repulsions compensate for the release of  $5s^2 > 5s^1$  coulomb energy, and for Ru and Rh, their IEs are greater than the -E(5s)as favorable exchange factors lessen for  $d^n$  (n > 5) and C(4d) coulomb energies become pronounced at contracted  $r_{12}$ . Pd is an outlier in this row as ionization from the neutral GS 4d10 configuration at 804.4 kJ/mol is higher than expected from the Y-Rh trend. Most of this energy is due to ionization from the lower-energy 4d orbital (-E(4d) = 924.3 kJ/mol), but the energy difference is attenuated somewhat by relief from Coulomb repulsions (by C and 4C') in the cation, despite its smaller  $r_{12}$ . It is crucial to realize that the *importance of Pd in Pd*<sup>0</sup>/ Pd<sup>II</sup> organometallic transformations stems from its relative ease of reduction, and this property is elemental!<sup>31-33</sup> There is no difference between the IE of Ag, and its -E(5s), which is 5 eV above the E(4d); apparently loss of this electron incurs little change in the 4d<sup>10</sup> configuration energy from neutral to cation. For Cd, E(5s) is 9 eV above E(4d), and the PES predicts the IE

II.B.6. Third-Row TM IEs. As Figure 11 reveals, the 5d and 6s orbitals are quite similar in energy for the third row (Figure 6b,

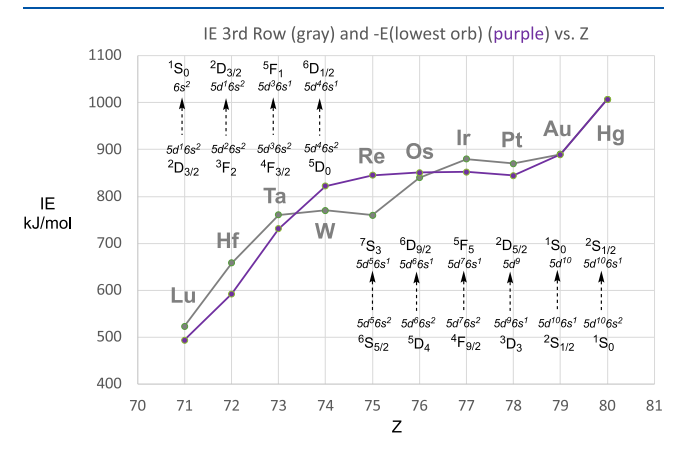


Figure 11. Plots of IE (gray, kJ/mol) and -E of the low-valence orbital (purple, kJ/mol) from PES for the third row of the transition elements. Electron configurations and states (NIST) are given for the  $M^0$  (g) (below) and  $M^+$  (g) (above).

 $\Delta E = \pm 1.8$  eV for Lu–Pt), and the 5d is the highest *E* orbital for Lu, Hf, and Ta. Ionizations from 5d occur for Lu and Hf, and the IEs for the three are higher than the -E(5d) energies, perhaps due in part to loss of favorable exchange factors ((-K + 2C')) for Hf; -3(-K + 2C') for Ta), and energy considerations from contraction of  $r_{12}$  in the cations. The 5d orbital drops below 6s at W, and the PES data does a good job of matching the IE trend, with Re as the worst case, where relief of a Coulombic repulsion from 6s helps render the IE lower in energy by ~85 kJ/mol. From Os to Hg, arguments related to those applied to the second-row TMs can be made, as ionizations occur from the 6s<sup>2</sup> for Os and Ir. The unique 5d<sup>9</sup>6s<sup>1</sup> configuration for Pt suggests occupation of a lower energy 5d orbital ( $\Delta E(5d-6s) \sim -1.8$ eV) is preferred over the Coulombic repulsion in 6s, rendering IE and -E(6s) very close. Au and Hg  $5d^{10}$  occupations are apparently unaffected by ionization as the match of IE and -E(6s) is excellent.

The most interesting factor is the big increase in IE energies for the third row over the first and second rows due principally to poor screening by occupied 4f<sup>14</sup> electrons, i.e., the kainosym-

metric effect more commonly known as the lanthanide contraction. There are subtle relativistic factors that are partly responsible for the low energies of 6s orbitals, complicating a discussion of the third row that already requires the assessment of many parameters, rendering the arguments quite tentative.

It is expected that as  $e^2/r_{12}$  factors diminish descending the table, because  $r_{12}$  (3rd row)  $\geq r_{12}$  (2nd row)  $> r_{12}$  (1st row), the match of IE with -E(low orb) (i.e.,  $\Delta E = \text{IE} - (-E(\text{low orb}))$ ) should be better, and this is supported by the data, but care must be taken in evaluating the  $\Delta E$  numbers. Evaluating  $\Delta E_{\text{RMS}} = [1/10\{(\Delta E_1)^2 + (\Delta E_2)^2 + ... (\Delta E_{10})^2)]^{1/2}$ , the root-mean-square of the variations, the first (Sc-Ni), second (Y-Pd), and third (Lu-Pt) rows are 37, 39, and 32 kJ/mol, respectively, clearly indicative of *similar magnitudes in variation*. However, the average variation in the first, second, and third rows are -34, -2, and 4 kJ/mol, respectively, revealing that the orbital energy differences are on par with Coulombic and exchange factors for the second and third rows. It is apparent from the basic analyses above why freshman textbooks avoid scrutinizing the TMs aside from providing electron configurations.

II.B.7. Points of Emphasis: TM Oxidation. 1) IEs generally increase across each row, as Zeff increases. 2) Poor screening by the kainosymmetric 3d orbitals renders IEs of the second-row TMs similar to those of the first-row. 2) Poor screening by the kainosymmetric 4f orbitals (the lanthanide contraction) renders IEs of the third-row TMs relatively higher. 3) Aside from Y, Lu, Hf, and Ta, the nd orbitals are below the (n+1)s orbitals in each row. 4) Orbital energies obtained (vertical ionizations) primarily differ from IEs (adiabatic) due to various interactions: unfavorable Coulombic and favorable exchange energies. Pairwise interactions are a means of examining the differences, but since the neutral and cationic species interact at a different distance  $(r_{12})$ , even simple assessments are difficult. 5) As one descends the periodic table, nd and (n+1)s orbitals become closer in energy, and ns/(n+1)d mixing, which is consequential in assessing the electronic structures in coordination/organometallic chemistry, has an elemental origin.

II.C. Elemental Reduction. II.C.1. Electron Affinities. Herein, the electron affinity (EA) is defined as the energy change occurring from attachment of an electron to the neutral X(g), hence EA < 0 is favorable, but in Figure 12, —EA vs Z is plotted for convenience. The ground-state configurations of the neutral and anionic ( $Z^-$ ) elements can again be assessed in terms of

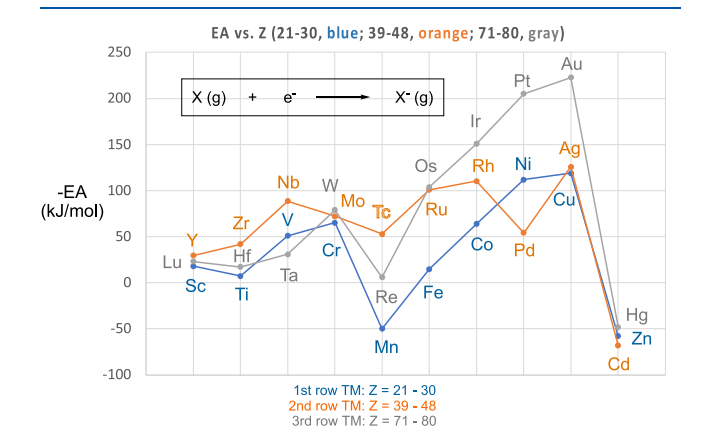


**Figure 12.** Electron affinities ( $\Delta E = EA$ ) as defined for the formation of  $X^-$  (g) as shown in the equation above, here plotted as -EA vs Z (-EA > 0 is favorable) for the 1st (blue), 2nd (orange), and 3rd (gray) row TMs.

 $E(\rm ns), E(\rm nd), C, C', and \pm K,$  but less reliable information is available for orbital energies of the anions, and  $\rm r_{12}$  changes are likely even more problematic. What is obvious are the relative magnitudes of the EAs, which are on average 10–20% those of the IEs.

Since less information is available, a cursory look at the rows will suffice. In general, the EAs of the TMs decrease (-EA increases) across the table as Zeff increases due to poorer screening, the same general effect observed for IEs. There is a break in the trend at  $(nd)^5((n+1)s)^2$ , where the addition of an electron causes the first 3d coulomb interaction (C). Consequently, anion formation is unfavorable where  $r_{12}$  is small for first row Mn (g), essentially energetically neutral for third-row Re (g), and only modestly favorable for second-row Tc (g). For configurations [(nd)((n+1)s)] containing 8–11 electrons, the third-row transition elements have more favorable EAs than the first-row TMs by  $\sim$ 100 kJ/mol consistent with an additional C compulsory with each additional electron over larger  $r_{12}$  in the anions. The second-row TMs are again modest outliers to the trend, presumably a consequence of the relatively similar 4d orbital energies, as expounded upon in the discussion of IEs in Figure 10. Poor screening by the (n+1)s orbital enables the EAs to be quite favorable for Cu, Ag, and Au, and the unfavorable EAs for group 12 reflect electron additions to closed-shell species.

II.C.2. Electronegativities. Certain elemental properties that are not measurable quantities can often be valuable in terms of chemical insight. Electronegativity (EN) is arguably the most consequential of such properties, as the vernacular of inorganic and organometallic chemistry is laced with concepts of electron density being donated or accepted. Various electronegativities have been invented (i.e., Mulliken, Allred–Rochow, Allen, Rahm–Hoffmann, and Sanderson), and they are typically scaled to Pauling's initial approach. Sanderson's method is a cornerstone of electronegativity equalization, which can be used to calculate simple molecular geometries and other properties, as electrons are considered distributed in a molecule due to electronegativity minimalization.

While an electronegativity construct involving IE and EA (e.g., Mulliken) is perhaps the most logical, most freshman textbooks still defer to Pauling,  $^{11}$  and this treatise will also. Roughly defined as "the ability of an atom in a molecule to attract shared electrons to itself", electronegativity is rooted in experiment, as a parametrization of " $\Delta$ ", the difference between experimentally determined dissociation energies, D(AB), of the heterodiatomic molecule AB (g), and the average of D(AA) and D(BB), the respective experimental numbers of the homolytic  $\rm A_2$  and  $\rm B_2$  molecules ( $\rm \Delta = D(AB) - \{D(AA) + D(BB)\}/2)$ . The chosen range of electronegativity  $\rm X_A$  or  $\rm X_B$  from 0.7 to -4.0 was likely one of convenience as regression analyses of the data set afforded fits to  $\rm \Delta \sim 96.5~kJ/mol~(X_A - X_B)^2$ .

Most chemists are quick to provide the "lower left to upper right" sweeping reference to the trend in ENs, but the TMs belie this generalization pertinent to the MG. While groups 3–5 appear to conform, groups 6–12 are virtually opposite, with lower values in the first row, and the second- and third-row elements becoming increasingly electronegative as the concept of shared electrons becomes more relevant for species with a greater capacity for covalency (Figure 13, Figure 14 inset). Once again, primary occupation of the contracted 3d orbitals (the kainosymmetric effect), and its consequence of poor shielding,

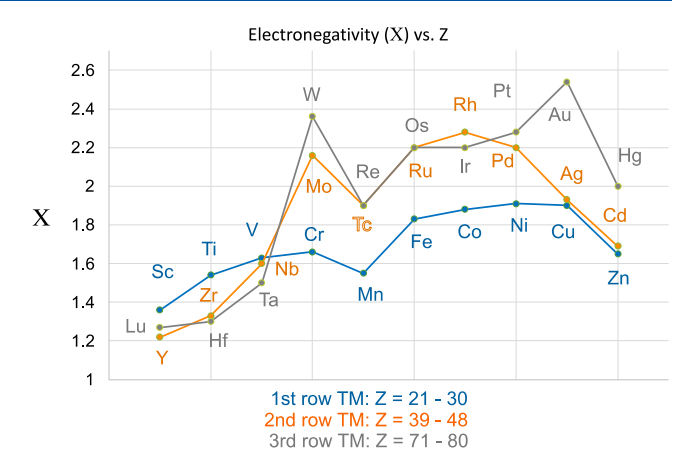


**Figure 13.** Pauling electronegativities (EN, X) plotted vs Z for the 1st (blue), 2nd (orange), and 3rd (gray) row TMs.

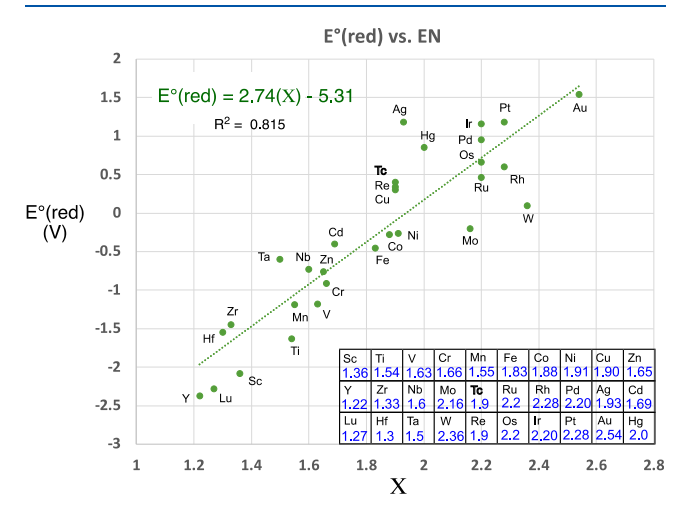


**Figure 14.** Plot of aqueous TM reduction potentials  $(M^{n+} + ne^- \rightarrow M)$ , as defined in the key to Figure 4, vs Pauling electronegativites (X), with the inset tabulating the values.

renders the first-row TMs more ionic in character than their 4d and 5d congeners.

*II.C.3. Reduction Potentials:* E°(red) vs EA. In viewing periodic properties of the TMs, a correlation of electronegativity with electron affinity, EA, might be expected (it is poor). Since electronegativities are defined by how electrons are shared in chemical bonds, a better correlation is realized when X values are plotted relative to the various aqueous reduction potentials<sup>36</sup> as defined in Figure 4 and shown in Figure 14. While redox potentials are clearly not "elemental", some bending of these rules are important as intrinsic information regarding the elements may be construed. The ease of reduction should correlate to higher EN values, as is observed, and there is a modest amount of scatter about the  $E^{\circ}(\text{red}) = 2.74\text{X} - 5.31$ trendline. First-row elements undergoing 2e reductions lie below the line, as do multielectron (>2) reductions of the early metals, whereas reductions involving oxidic species and late metal second- and third-row reductions occur above the line, so speciation is a factor.

II.C.4. Reduction Potentials:  $E^{\circ}(red)$  vs IE. If the transition metal is intrinsically difficult to ionize, it should be easier to reduce. In Figures 5 and 9–11, transition metal ionization energies were found to increase as third row > second row ~ first row and increasing within the rows as Z increases. The few

outliers are in the early transition metals, but the trends were otherwise quite general. Figure 15 shows that there is a

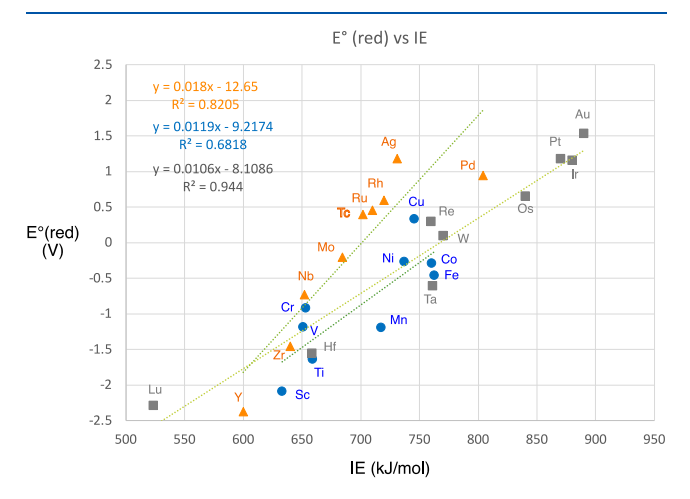


Figure 15. Plot of aqueous TM reduction potentials  $(M^{n+} + ne^- \rightarrow M)$ , separated by TM row, as defined in the key to Figure 4, vs ionization energies (IEs, kJ/mol).

significant trend of  $E^\circ(\text{red})$  with IE as expected. The most electronegative elements that coincide with the most positive  $E^\circ(\text{red})$  values correlate strongly with IE. While it would be interesting to apply additional factors, like solvation energies  $(\Delta H^\circ_{\,\,\mathrm{f}} \, (\text{solv}(aq)))$  and heats of sublimation  $(\Delta H^\circ_{\,\,\mathrm{f}} \, (g))$  as in Figure 2 to further refine the interrelationship, there are numerous complications, such as second  $(M^+\,(g)\to M^{2+}\,(g)+e^-)$  and third  $(M^{2+}\,(g)\to M^{3+}\,(g)+e^-)$  ionization energies, speciation in aqueous solution, etc.

For example, heats of sublimation show a smooth trend for alkali metals, but the metal—metal bonding in solid elemental TMs manifests as highly variable  $\Delta H^{\circ}_{\rm f}$  (g)'s ( $\Delta H^{\circ}({\rm vap})$ 's), as shown in Figure 16. It is not clear what solvation factors may or may not compensate for this variation. Second IEs (i.e.,  $M^{+} \rightarrow M^{2+} + e^{-}$ ) vs  $E^{\circ}({\rm red})$  show a relatively similar trend with a modest increase in scatter, so at least it appears that the correlation with first ionization energy is relevant, even for those multiple-electron reductions. As Figure 15 illustrates, slopes of  $\Delta(E^{\circ}({\rm red})/\Delta({\rm IE}))$  are similar for the first and third rows, but

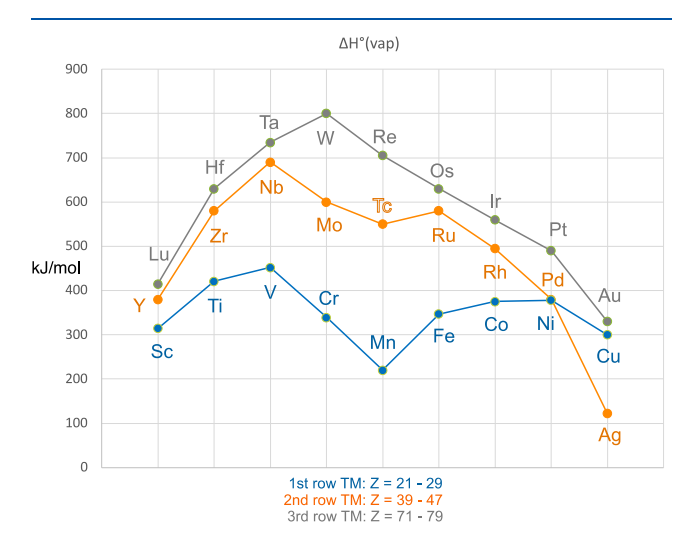


Figure 16. Heats of vaporization  $(\Delta H^{\circ}(\text{vap}))$  for selected transition metals (kJ/mol).

there is appreciably more scatter in the trendline for the first row, reflecting variation in IEs. IE values for the second and third rows increase in a more regular fashion, hence the correlations are smoother, but the slope of the second-row correlation is >50% greater than the other two rows. Both the second and third rows have a nearly 4.0 V range in  $E^{\circ}(\text{red})$ , but the former has roughly half the IE range, hence the slope difference. Alternatively stated, the greater range in third-row IEs does not translate into a greater range in  $E^{\circ}(\text{red})$  values. Clearly, the heats of vaporization, the multiple ionization energies, and solvation enthalpies provide a complicated landscape for full analysis of reduction potential.

II.C.5. Reduction Potentials: Frost Diagrams. The Frost diagrams<sup>37,38</sup> shown in Figure 17 are a means of assessing relative free energies of compounds with respect to assigned formal oxidation states (FOSs). The data are chosen relative to a specific reference potential, which is usually the standard hydrogen electrode (SHE) common in most data compilations. While speciation now becomes a significant factor in terms of the actual aqueous species (1 M), the trends provide an additional indication of their elemental character. Of special interest are the minima displayed in the  $\Delta G^{\circ}/F$  lines pertaining to the first-row TMs, except for Ti and Cu, and the corresponding smoothness of the lines attributed to the second- and third-row TMs. Relative redox values are a measure of chemical potential (internal energy), but FOSs are a bookkeeping construct, and are not measurable. Minima in the Frost diagrams are likely a consequence of a greater ionic contribution to stability in some of the first-row TM elements, particularly octahedral M- $(OH_2)_6^{2+}$  (M = V-Ni) species. As the greater variety in speciation occurs, covalency in the form of metal-oxygen multiple bonding smooths the lines, and it is notable that in the middle of the periodic table, in particular group 6, the FOSs of Mo or W have no bearing on chemical potential. Noteworthy in this respect is the ability of aquo complexation to distribute charge in simple aquo species, i.e.,  $M(OH_2)_6^{n+}$ .

Figure 18 provides a direct comparison between the rows for groups 6 and 7, highlighting the stability of Cr3+ and Mn2+ relative to their higher conjugates in 1 M acid. In group 7, the slopes of the  $\Delta(\Delta G^{\circ}/F)/\Delta FOS$ s lines tend toward convergence at high FOS, an indication that the first row TMs become more covalent with increasing FOS. Similar trends can be seen by scanning the Frost diagrams in Figure 17, and the data suggest that the first-row TMs have a clear ionic nature as formal 2+/3+species, but that is a limiting character that rapidly dissipates with increasing FOS. The data also speaks to FOSs as a conceptual problem. One could argue that the ~7 V change accorded FOSs of Mn<sup>2+</sup> (II) to MnO<sub>4</sub> - (VII) has some meaning, but each FOS change upon traversing W(0) to  $WO_3(VI)$  is less than 0.8 V, and the two extremes differ by  $\sim$ 0.5 V. Mo is similar in nature, while Cr is the only group 6 metal that manifests significant changes with FOS. If one persists in assigning chemical potential to formal oxidation states, note that Figure 18c shows that the  $\Delta G^{\circ}/F$  dispersion is a factor of the pH dependence of the redox potentials combined with speciation. The medium, in this case 1 M base, helps provide electron density to the metal center, and the real chemical potential of species with differing formal oxidation states is quite modest.

II.C.6. Points of Emphasis: TM Reduction. 1) Information on TM anions is limited, and the inability to assess their orbital, Coulombic, and exchange energies renders any discussion of electron affinities difficult. There is a modest increase in favorable energy across a row, as nd screening is less effective. 2)

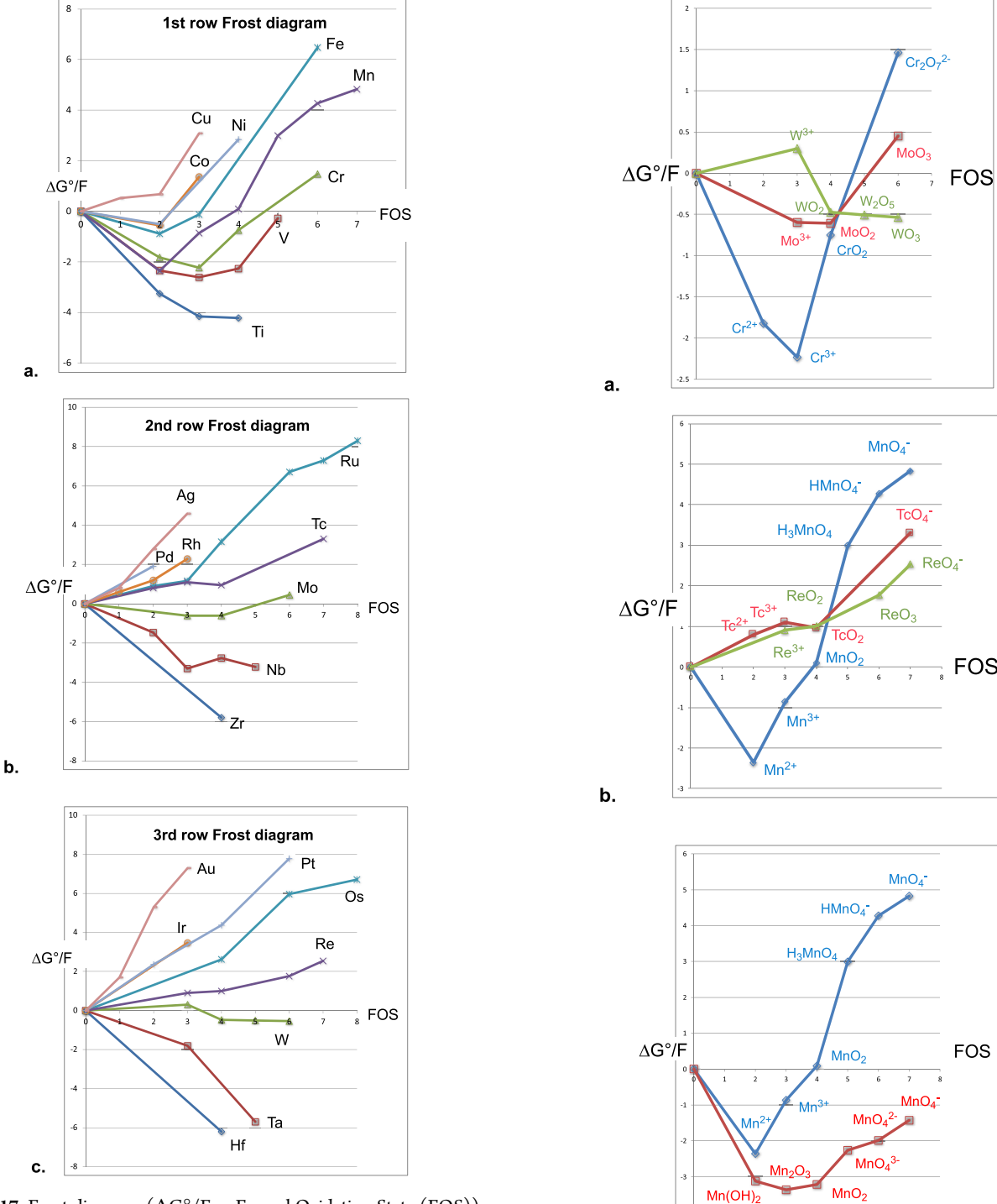


Figure 17. Frost diagrams ( $\Delta G^{\circ}/F$  vs Formal Oxidation State (FOS)) under standard state (aqueous, all solutes 1 M, referenced to SHE) conditions for the 1st (a.), 2nd (b.), and 3rd (c.) row TMs.

Electronegativity is a valuable construct for TMs, and in groups 6-10, X values run counter to MG trends in that third row > second row > first row. Second- and third-row TM values even approach those of MG rows 14 and 15. 3) ENs correlate with  $E^{\circ}$  (red) values, and suggest first-row TMs are substantially more ionic than their congeners. 4) Ease of reduction ( $E^{\circ}$  (red) increasingly positive) tracks with an increase in IEs, and the correlation is most pronounced in the third row. 5) Frost diagrams suggest that the first-row TMs have ionic character, and that the second- and third-row TMs are relatively covalent.

**Figure 18.** Comparative Frost diagrams ( $\Delta G^{\circ}/F$  (red) vs Formal Oxidation State (FOS)) under standard state (aqueous, 1 M) conditions for groups 6 (a.) and 7 (b.). (c.) Comparison of 1 M acid (blue) and 1 M base (red) conditions for manganese. *Note the ordinate* (*y-axis*) for the three charts are scaled differently.

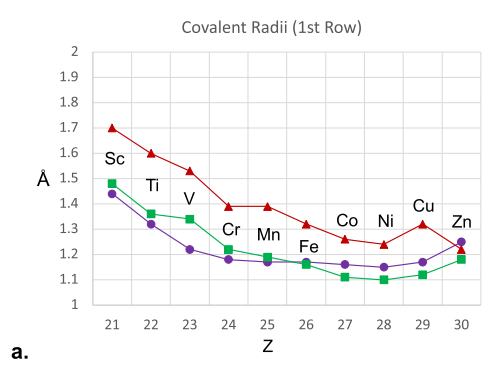
- 6) Redox potentials are highly dependent on speciation and medium, and often do not show much change in chemical potential with FOSs.
- D. Covalent Radii. The last topic usually covered in an introductory text regarding the periodic table is a compilation of radii: atomic, van der Waals, ionic, metallic, and covalent. Immediately, one is confronted with discerning which radius is

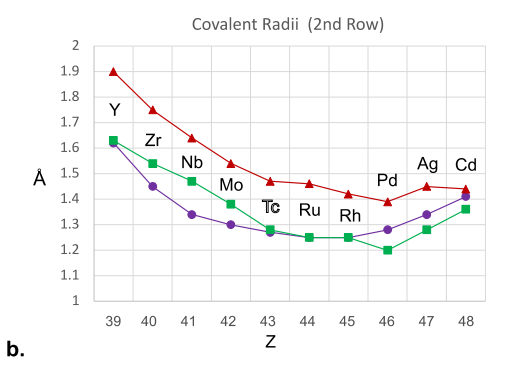
C.

most relevant to the organometallic chemist. While the minimum contact of two nonbonding atoms, the van der Waals radius, is becoming increasingly important as the effects of dispersion are being recognized,<sup>39</sup> the rationalization of bond distances is probably the most crucial factor of interest, especially to the organometallic chemist. Consequently, the periodic table in Figure 4 features Pauling covalent radii (c<sub>r</sub>), which are typically found on commercial periodic tables. Given the enormous amount of crystallographic data, and the resulting compilation of distances, 40 one can now look up a value related to the bond of interest. In terms of closest nonbonding contacts, Echeverria and Alvarez have interpreted a van der Waals "crust" with respect to its interpenetration in pairs of atoms. They have explored a host of compounds in great detail and, while beyond the scope of this tutorial, have provided a valuable and interesting perspective of bonding and nonbonding interactions.41

From a pedagogical standpoint, it is still important to have a ballpark idea of a bond length for classroom conversation and rough interpretation, but what are the radii of choice? Radii are often described by the nebulous term "size", probably due to the heresy in selecting one set of c, over another, but it is likely that your commercial periodic table still features Pauling radii, 5and Figure 19 illustrates these, along with more modern versions from Pyykkö<sup>7</sup> and Alvarez,<sup>6</sup> which is a set derived from experimental data found in the Cambridge Crystallographic Database. Since predictions of a bond length within  $\sim$ 0.05 Å are desired, the discrepancy between the sets in all rows is not particularly comforting, but there are some generalities. From left to right on the table, the increase in Z<sub>eff</sub> manifests in a shortening of c<sub>r</sub>, but there is an uptick nearing the end of each row as repulsion from the number of e- actually increases screening. The Pauling radii are the easiest to memorize, as they change from Sc (1.44 Å) to Ti (1.32 Å) to V (1.22 Å) by 0.10 Å, then by 0.05 to Cr (1.18 Å), and essentially remain the same  $(\pm 0.02 \text{ Å})$  across the row until the uptick at Zn (1.25 Å). In groups 11 and 12, there is essentially an increase of 0.10(3) Å upon moving to the second row, except for a greater uptick near the end, and the third row is essentially the same as the second because of the lanthanide contraction. The trends tend to jive with the Pyykkö numbers, which tend to be significantly greater for the early metals, and modestly less for the later metals, relative to Pauling's values. Anecdotally, the c<sub>r</sub> extracted from Xray structural data from these laboratories is often in between the Pauling and Pyykkö numbers, and either is a decent start for a rough estimation. Pyykkö's compilation has the advantage of listing double and triple bond radii. The Alvarez numbers undoubtedly are derived from a collection of distances that include coordination chemistry, and appear relatively long for organometallic applications, presumably due to inclusion of weaker field compounds.

E. Formal Oxidation States and the Opposite Extreme, Charge States (c(TM)). Throughout this treatise, the reader will have noticed an emphasis on FOSs as bookkeeping factors and clearly not measurable properties. While important in categorizing reactivity, especially in organometallic chemistry, FOSs are bereft of reality in terms of actual charge. FOSs are an extreme view that mandates integer charges based on closed-shell configurations of ligands. In the ionic limit, FOS values would be realistic, but Pauling showed many years ago that no compound, not even simple AB (g) species such as salts, is devoid of covalency. Since most species are viewed via Molecular Orbital Theory (MOT), the idea that charges on





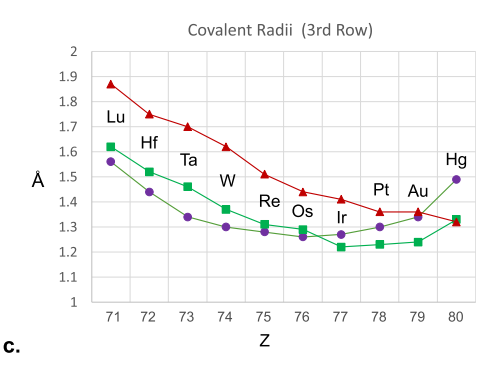


**Figure 19.** Three types of covalent radii for the first (a.), second (b.) and third (c.) rows: 1) Pauling (purple circle);<sup>3–5</sup> 2) Pyykkö (green square);<sup>7</sup> 3) Cambridge Structural Database (Alvarez, red triangle).<sup>6</sup>

atoms must be integers is recognized as antiquated, and the means by which partial charges are assigned is method dependent. Any high level calculational method—MOT, Valence Bond Theory (VBT), Density Funtional Theory (DFT), etc.—relies on method-dependent partitioning of charge (e.g., Natural Bond Orbital Analysis (NBO), Mulliken) that leads to fractional charges. Charge Distribution Via Reporters (CDVR) is a desktop method based on  $[M(CO)_x]^p$  stretching frequencies. Metal charge states (c(TM)) are derived from the correlation of v(CO) (ave) of  $\sim 100$  carbonyl complexes with charge, and are assigned relative to a  $c_{Fe} = +2.0$  reference state, as detailed elsewhere. The c(TM) are single values for the charge of a TM that is the opposite extreme of variable FOSs.

Older periodic tables (and some current) often listed common oxidation states; c(TM) values are surprisingly close to an "average" of those FOSs listed for each element. The charge state number can be considered a core value reflecting the intrinsic electropositive nature of the metal, and a correlation with K-edge energies (XAS:  $1s \rightarrow continuum$  (ejection of a 1s electron)) of each TM(s) is clearly manifested, as shown in

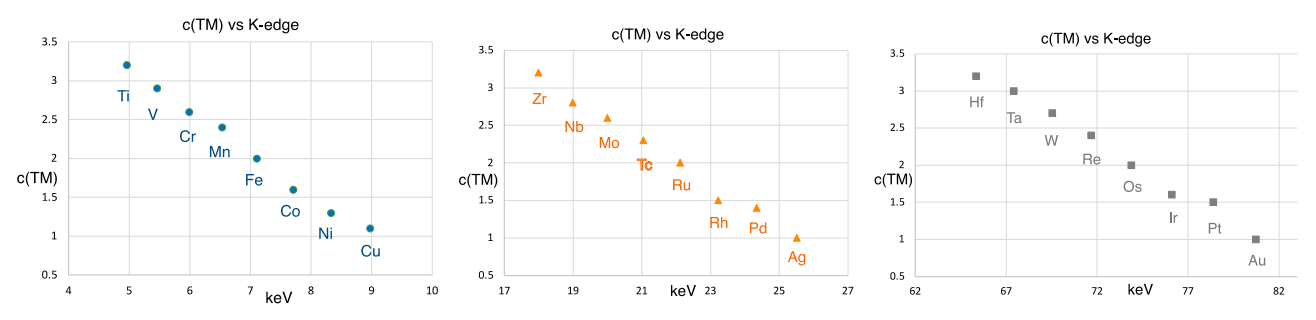


Figure 20. CDVR charge values  $(c(TM))^{22}$  correlated with K-edge (1s  $\rightarrow$  continuum) XAS values (in keV) of each TM(s).

Figure 20. The easier it is to eject a core electron coincides with a higher c(TM) value, i.e., the more electropositive the metal behaves. It is interesting that as Z increases, and the energy needed to eject a core 1s electron increases substantially, charge values via CDVR do not change among the rows. Compensatory screening renders each group as having roughly a common c(TM). It is noteworthy that high-energy spectroscopic investigations of late first-row TMs show a surprisingly decent correlation between c(TM) and corresponding  $d^n$  count.  $d^{45-48}$ 

F. Bond Dissociation Free Energies of Aquo Complexes. While the primary focus of this tutorial has been elemental, aspects of aquo complex ion reduction potentials seemed appropriate since electron affinities are not particularly informative, but having some understanding of reduction is critical. Moreover, the correlation of  $E^{\circ}(\text{red})$  values with electronegativity (Figure 14) and ionization energies (Figure 15) shows how elemental properties translate into chemical reactivity.

As an extension of reduction, examination of metal aquo complexes in the context of proton-coupled electron transfer (PCET) deserves some consideration. There is a limited amount of data regarding the p $K_a$ s of  $[M(OH_2)_6]^{n+}$  (n = 2, 3),  $^{49-52}$  but there is enough to assess the bond dissociation free energies (BDFEs) indicated in eq 1 via the expression for BDFE shown in eq 2.  $^{53,54}$  Using both measured and

$$[M(OH_2)_6]^{n+} \rightarrow [M(OH_2)_5(OH)]^{(n-1)+} + H^{\bullet}$$
 (1)

BDFE (in kcal/mol) = 
$$(1.37)pK_a + (23.06)E_{red}^{\circ} + 52.8$$
 (2

calculated p $K_a$  values, Figure 21 shows how the reduction potential dominates the BDFE. The data is limited to mostly first row TM, but a few second row aquo complexes are known:  $[Mo(OH_2)_6]^{3+}$ , BDFE (estimated) = 48 ( $E^{\circ}(red) = -0.2$ );  $[Ru(OH_2)_6]^{3+}$ , BDFE = 62.5 (p $K_a$  = 2.9,  $E^{\circ}(red)$  = 0.249);  $[Rh(OH_2)_6]^{3+}$ , BDFE = 82.2 (p $K_a$  = 3.4,  $E^{\circ}(red)$  = 1.07).

It is important to note that the high-oxidation-state species of first-row TMs have high BDFEs, and hydrogen atom transfer (HAT) chemistry has been observed with many of these elements. So-called Cu(III) has been shown to have considerable "hole" character on the ligands, <sup>45</sup> Co(III)/Co(II) and Mn(III)/Mn(II) couples are crucial to autoxidation processes such as the autoxidation of *p*-xylene to terphthalic acid, <sup>55</sup> and myriad iron species, including critical bioinorganic species like cytochrome P450 <sup>56</sup> have been shown to exhibit HAT. <sup>53,54</sup> It appears from this abbreviated correlation that the ability to do reactions featuring OH bond-making or -breaking are intrinsic to the metals. As a consequence, the extensive ligand design surrounding these metals features encapsulation and

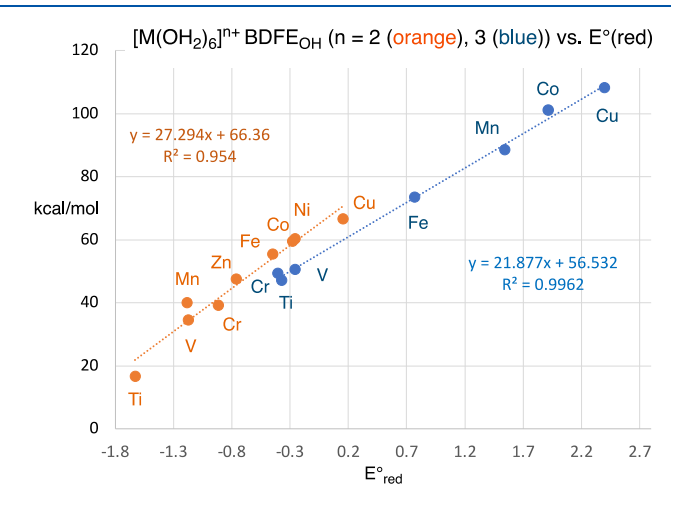


**Figure 21.** BDFEs pertaining to OH bonds of  $[M(OH_2)_6]^{2+}$  (orange) and  $[M(OH_2)_6]^{3+}$  (blue) calculated according to BDFE (in kcal/mol) =  $(1.37)pK_a + (23.06)E^{\circ}_{red} + 52.8$ .

protection of the reactive metal center and not a large redox change.

G. Conclusions. Hopefully, the discourse above can serve as an introduction to an advanced undergraduate or first-year graduate course that emphasizes transition metals. If there is an overarching point to this tutorial, it is that the electronic complexity of transition elements is important, and translates to complexation and reactivity. If there is any question that elemental properties have significant consequences, look no further than the outlying (high) IE of Pd, which strongly suggests that its use in Pd<sup>2+</sup>/Pd<sup>0</sup> catalytic cycles is predicated on its ease of reduction. In addition (n+1)s/nd orbital mixing that occurs to a greater extent in the third row is elemental in origin. It is also clear that even heteroatom CH bond activation by first row TMs has an intrinsic, elemental origin. Electron configurations of the TMs may be found in freshman textbooks, but the underlying energy considerations are rarely delineated, even in advanced inorganic/organometallics courses. Hopefully the reader will find the discussions of orbital and Coulombic repulsions useful, and can spot how they translate to complex ion spectroscopy and chemical reactivity.

# ASSOCIATED CONTENT

# Supporting Information

The Supporting Information is available free of charge at https://pubs.acs.org/doi/10.1021/acs.organomet.3c00529.

Numerical values for Figure 3 (PDF)

Excel spreadsheet containing the data used in the Figures (XLSX)

#### AUTHOR INFORMATION

# **Corresponding Author**

Peter T. Wolczanski – Department of Chemistry & Chemical Biology, Baker Laboratory, Cornell University, Ithaca, New York 14853, United States; oorcid.org/0000-0003-4801-0614; Email: ptw2@cornell.edu

Complete contact information is available at: https://pubs.acs.org/10.1021/acs.organomet.3c00529

#### **Notes**

The author declares no competing financial interest.



Peter T. Wolczanski has spent nearly 50 years investigating the synthetic and mechanistic chemistry of inorganic and organometallic complexes, with a focus on electronic structural factors that influence reactivity. These endeavors often uncovered elemental origins underpinning the complexities, and this tutorial is a compilation of information that is sometimes overlooked or underappreciated. When not pushing the forefront of science, he can be found sampling the local lake water.

## ACKNOWLEDGMENTS

PTW thanks the National Science Foundation for funding this work (CHE-1953884), and the support of Cornell University. Profs. Clifford P. Kubiak, S. Figueroa, and the Univ. California San Diego chemistry department are acknowledged for providing sabbatical leave support during the initiation of this project. Most data was taken from NIST (webbook.nist.gov/chemistry/; NIST: Atomic Spectra Database). It is important to note that in the database, M (I) actually refers to a neutral metal, M<sup>0</sup>; M (II) refers to M<sup>I</sup>; M (III) refers to M<sup>II</sup>, etc. PTW would like to thank the following colleagues for critical discussion: Profs. Roald Hoffmann, Melissa A. Hines, and Kyle M. Lancaster (Cornell), Prof. Aaron Odom (Michigan State), Prof. James M. Mayer (Yale), and Thomas R. Cundari (North Texas).

#### REFERENCES

- (1) (a) Oxtoby, D. W.; Gillis, H. P.; Nachtrieb, N. H. Principles of Modern Chemistry; 4th ed., Brooks Cole: New York, 1998. (b) Pauling, L. General Chemistry; 2nd ed., W. H Freeman and Co.: San Francisco, 1954.
- (2) (a) Pfennig, B. W. Principles of Inorganic Chemistry; John Wiley & Sons: Hoboken, NJ, 2015. (b) Miessler, G. L.; Tarr, D. A. Inorganic Chemistry, 3rd ed.; Pearson Prentice Hall: Upper Saddle River, NJ, 2004
- (3) Hartwig, J. F. Organotransition Metal Chemistry; University Science Books: Mill Valley, CA, 2010.
- (4) Duncan, A. P.; Johnson, A. R.; Nataro, C. Literature-Based Teaching Strategies for Organometallic Courses. *Organometallics* **2017**, *36*, 2703–2705.
- (5) Pauling, L. The Nature of the Chemical Bond, 3rd ed.; Cornell University Press: Ithaca, N. Y, 1960.
- (6) Pauling, L. Atomic Radii and Interatomic Distances in Metals. J. Am. Chem. Soc. 1947, 69, 542–553.
- (7) (a) Pauling, L. Maximum-valence radii of transition metals. *Proc. Natl. Acad. Sci. U.S.A.* **1975**, *72*, 3799–3801. (b) Pauling, L. Covalence of atoms in the heavier transition metals. *Proc. Natl. Acad. Sci. U.S.A.* **1977**, *74*, 2614–2615. (c) Pauling, L. Metal-metal bond lengths in complexes of transition metals. *Proc. Natl. Acad. Sci. U.S.A.* **1976**, *73*, 4290–4293.
- (8) Cordero, B.; Gomez, V.; Platero-Prats, A. E.; Reves, M.; Echeverria, J.; Cremades, E.; Barragan, F.; Alvarez, S. Covalent radii revisited. *Dalton Trans.* **2008**, 2832–2838.
- (9) (a) Pyykkö, P.; Atsumi, M. Molecular Single-bond Covalent Radii for Elements 1–118. *Chem.—Eur. J.* **2009**, *15*, 186–197. (b) Pyykkö, P.; Atsumi, M. Molecular Double-bond Covalent Radii for Elements Li-E112. *Chem.—Eur. J.* **2009**, *15*, 12770–12779. (c) Pyykkö, P.; Riedel, S.; Patzschke, M. Triple-Bond Covalent Radii. *Chem.—Eur. J.* **2005**, *11*, 3511–3520.
- (10) Kepp, K. P. Free Energies of Hydration for Metal Ions from Heats of Vaporization. *J. Phys. Chem. A* **2019**, 123, 6536–6546.
- (11) (a) Pauling, L. The Nature of the Chemical Bond. IV. The Energy of Single Bonds and the Relative Electronegativity of Atoms. *J. Am. Chem. Soc.* **1932**, *54*, 3570–3582. (b) Pauling, L. The Origin and Nature of the Electronegativity Scale. *J. Chem. Educ.* **1988**, *65*, 375.
- (12) Mulliken, R. S. A New Electroaffinity Scale; Together with Data on Valence States and on Valence Ionization Potentials and Electron Affinities. *J. Chem. Phys.* **1934**, *2*, 782–793.
- (13) (a) Allred, A. L. Electronegativity Values from Thermochemical Data. J. Inorg. Nucl. Chem. 1961, 17, 215–221. (b) Allred, A. L.; Rochow, E. G. J. Inorg. Nucl. Chem. 1958, 5, 264–268.
- (14) Allen, L. C. Electronegativity is the average one electron energy of the valence-shell electrons in ground-state free atoms. *J. Am. Chem. Soc.* **1989**, *111*, 9003–9014.
- (15) Bratsch, S. G. Revised Mulliken Electronegativities. 1. Calculation and Conversion to Pauling Units. *J. Chem. Educ.* **1988**, 65, 34–41.
- (16) (a) Rahm, M.; Zeng, T.; Hoffmann, R. Electronegativity Seen as the Ground-State Average Valence Electron Binding Energy. *J. Am. Chem. Soc.* **2019**, *141*, 342–351. (b) Rahm, M.; Hoffmann, R. Toward an Experimental Quantum Chemistry: Exploring a New Energy Partitioning. *J. Am. Chem. Soc.* **2015**, *137*, 10282–10291.
- (17) (a) Sanderson, R. T. Principles of Electronegativity. 1. General Nature. *J. Chem. Educ.* **1988**, *65*, 112–118. (b) Sanderson, R. T. Principles of Electronegativity. 2. Applications. *J. Chem. Educ.* **1988**, *65*, 227–231.
- (18) Accorinti, H.; Labarca, M. Commentary on the Models of Electronegativity. *J. Chem. Educ.* **2020**, *97*, 3474–3477.
- (19) Kaupp, M. The Role of Radial Nodes of Atomic Orbitals for Chemical Bonding and the Periodic Table. *J. Comput. Chem.* **2007**, 28, 320–325
- (20) Kaupp, M. Chemical Bonding of the Main-Group Elements. In *The Chemical Bond: Fundamental Aspects of Chemcal Bonding*, Frenking, G.; Shaik, S., Eds., Wiley: New York, 2014.

- (21) Yao, B.; Kuznetsov, V. L.; Xiao, T.; Slocombe, D. R.; Rao, C. N. R.; Hensel, F.; Edwards, P. P. Metals and non-metals in the periodic table. *Philos. Trans. R. Soc. A* **2020**, *378*, No. 20200213.
- (22) Wolczanski, P. T. Flipping the Oxidation State Formalism: Charge Distribution in Organometallic Complexes as Reported by Carbon Monoxide. *Organometallics* **2017**, *36*, 622–631.
- (23) Jensen, W. B. The Place of Zinc, Cadmium, and Mercury in the Periodic Table. *J. Chem. Educ.* **2003**, *80*, 952–961.
- (24) Matsumoto, P. S. Trends in the Ionization Energy of Transition-Metal Elements. *J. Chem. Educ.* **2005**, 82, 1660–1661.
- (25) Jordan, R. B. Lanthanide Contraction: What is Normal? *J. Chem. Educ.* **2023**, *62*, 3715–3721.
- (26) Pyykkö, P. Relativistic Effects in Structural Chemistry. *Chem. Rev.* **1988**, 88, 563–594.
- (27) Periodic Table of Atomic Orbital Energies. *Chemiatria*. 2014. http://www.graylark.com/eve/orbital-energies-table.html.
- (28) Schwarz, W. H. E. The Full Story of the Electron Configurations of the Transition Elements. *J. Chem. Educ.* **2010**, *87*, 444–448.
- (29) Schwarz, W. H. E. Recommended Questions on the Road Towards a Scientific Explanation of the Periodic System of Chemical Elements with the Help of the Concepts of Quantum Physics. Foundations of Chemistry 2007, 9, 139–188.
- (30) (a) Hirsekorn, K. F.; Hulley, E. B.; Wolczanski, P. T.; Cundari, T. R. Olefin Substitution in (silox)<sub>3</sub>M(olefin) (silox = <sup>t</sup>Bu<sub>3</sub>SiO; M = Nb, Ta): The Role of Density of States in 2nd vs. 3rd Row Transition Metal Reactivity. *J. Am. Chem. Soc.* **2008**, *130*, 1183–1196. (b) Kuiper, D. S.; Douthwaite, R. E.; Mayol, A.-R.; Wolczanski, P. T.; Lobkovsky, E. B.; Cundari, T. R.; Lam, O. P.; Meyer, K. Molybdenum and Tungsten Structural Differences are Dependent on nd<sub>22</sub>/(n+1)s Mixing: Comparisons of (silox)<sub>3</sub>MX/R (M = Mo, W; silox = <sup>t</sup>Bu<sub>3</sub>SiO). *Inorg. Chem.* **2008**, *47*, 7139–7153.
- (31) (a) Suzuki, A. Cross-Coupling Reactions Of Organoboranes: An Easy Way to Construct C-C Bonds (Nobel Lecture). *Angew. Chem., Int. Ed.* **2011**, *50*, 6722–6737. (b) Negishi, E. Magical Power of Transition Metals: Past, Present, and Future (Nobel Lecture). *Angew. Chem., Int. Ed.* **2011**, *50*, 6738–6764. (c) Heck, R. F.; Nolley, J. P. Palladium-catalyzed vinylic hydrogen substitution reactions with aryl, benzyl, and styryl halides. *J. Org. Chem.* **1972**, *37*, 2320–2322.
- (32) (a) Martin, R.; Buchwald, S. L. Palladium-Catalyzed Suzuki-Miyaura Cross-Coupling Reactions Employing Dialkylbiaryl Phosphine Ligands. *Acc. Chem. Res.* **2008**, *41*, 1461–1473. (b) Surry, D. S.; Buchwald, S. L. Biaryl Phosphane Ligands in Palladium-Catalyzed Amination. *Angew. Chem., Int. Ed.* **2008**, *47*, 6338–6361. (c) Ruiz-Castillo, P.; Buchwald, S. L. Applications of Palladium-Catalyzed C-N Cross-Coupling Reactions. *Chem. Rev.* **2016**, *116*, 12564–12649.
- (33) (a) Hartwig, J. F. Transition Metal Catalyzed Synthesis of Arylamines and Aryl Ethers from Ayyl Halides and Triflates: Scope and Mechanism. *Angew. Chem., Int. Ed.* **1998**, 37, 2046–2067. (b) Hartwig, J. F. Evolution of a Fourth Generation Catalyst for the Amination and Thioetherification of Aryl Halides. *Acc. Chem. Res.* **2008**, 41, 1534–1544. (c) Culkin, D. A.; Hartwig, J. F. Palladium-Catalyzed a-Arylation of Carbonyl Compounds and Nitriles. *Acc. Chem. Res.* **2003**, 36, 234–245.
- (34) (a) Mortier, W. J.; Leuven, K. U. Electronegativity Equalization and Its Applications. *Struc. Bond.* **1987**, *66*, 125–143. (b) Mortier, W. J.; Ghosh, S. K.; Shankar, S. Electronegativity-equalization method for the calculation of atomic charges in molecules. *J. Am. Chem. Soc.* **1986**, *108*, 4315–4320. (c) Mortier, W. J.; Vangenechten, K.; Gasteiger, J. Electronegativity equalization: application and parameterization. *J. Am. Chem. Soc.* **1985**, *107*, 829–835.
- (35) Zhongzhi, Y. Electronegativity Equalization. *Prog. in Chem.* **2012**, 24, 1038–1049.
- (36) Electrochemical Series. In CRC Handbook of Chemistry and Physics, Rumble, J. R., Ed., CRC Press: New York, 2023.
- (37) Frost, A. A. Oxidation Potential-Free Energy Diagrams. J. Am. Chem. Soc. 1951, 73, 2680–2682.
- (38) Dutton, K. G.; Lipke, M. C. Correcting Frost Diagram Misconceptions Using Interactive Frost Diagrams. *J. Chem. Educ.* **2021**, 98, 2578–2583.

- (39) (a) Liptrot, D. J.; Power, P. P. London dispersion forces in sterically crowded inorganic and organometallic molecules. *Nature Rev. Chem.* **2017**, *1*, 2397–3358. (b) Mears, K. L.; Power, P. P. London Dispersion Effects on the Stability of Heavy Tetrel Molecules. *Chem.*—*Eur. J.* **2023**, *29*, e202301247. (c) Mears, K. L.; Power, P. P. Beyond Steric Crowding: Dispersion Energy Donor Effects in Large Hydrocarbon Ligands. *Acc. Chem. Res.* **2022**, *55*, 1337–1348.
- (40) (a) Allen, F. H.; Kennard, O.; Watson, D. G.; Brammer, L.; Orpen, A. G.; Taylor, R. Tables of Bond Lengths determined by X-ray and Neutron Diffraction. Part 1. Bond Lengths in Organic Compounds. *J. Chem. Soc. Perkin Trans. II* 1987, S1–S19. (b) Orpen, A. G.; Brammer, L.; Allen, F. H.; Kennard, O.; Watson, D. G.; Taylor, R. Tables of Bond Lengths determined by X-Ray and Neutron Diffraction. Part 2. Organometallic Compounds and Co-ordination Complexes of the d- and f-Block Metals. *J. Chem. Soc., Dalton Trans.* 1989, S1–S83.
- (41) Echeverria, J.; Alvarez, S. The borderless world of chemical bonding across the van der Waals crust and the valence region. *Chem. Sci.* **2023**, *14*, 11647–11688.
- (42) (a) Parkin, G.; Green, M. L. H. Application of the Covalent Bond Classification Method for the Teaching of Inorganic Chemistry. *J. Chem. Educ.* **2014**, *91*, 807–816. (b) Parkin, G. Valence, Oxidation Number, and Formal Charge: Three Related but Fundmentally Different Concepts. *J. Chem. Educ.* **2006**, *83*, 791–799.
- (43) (a) Weinhold, F.; Landis, C. R. Discovering Chemistry with Natural Bond Orbitals; Wiley: Hoboken, NJ, USA, 2012. (b) Glendening, E. D.; Landis, C. R.; Weinhold, F. Wiley Interdisciplinary Reviews Computational Molecular Science 2012, 2, 1–42. (c) Glendening, E. D.; Landis, C. R.; Weinhold, F. J. Comp. Chem. 2013, 34, 1429–1437. (d) Weinhold, F. J. Comp. Chem. 2012, 33, 2363–2379. (e) Weinhold, F. J. Comp. Chem. 2012, 33, 2440–2449.
- (44) Mulliken, R. S. Electronic Population Analysis on LCAO-MO Molecular Wave Functions. *J. Chem. Phys.* **1955**, 23, 1833–1840.
- (45) (a) DiMucci, I. M.; Lukens, J. T.; Chatterjee, S.; Carsch, K. M.; Titus, C. J.; Lee, S. J.; Nordlund, D.; Betley, T. A.; MacMillan, S. N.; Lancaster, K. M. The Myth of d<sup>8</sup> Copper(III). *J. Am. Chem. Soc.* **2019**, 141, 18508–18520. (b) Walroth, R. C.; Lukens, J. T.; MacMillan, S. N.; Finkelstein, K. D.; Lancaster, K. M. Spectroscopic Evidence for a 3d<sup>10</sup> Ground State Electronic Configuration and Ligand Field Inversion in [Cu(CF<sub>3</sub>)<sub>4</sub>]<sup>1-</sup>. *J. Am. Chem. Soc.* **2016**, 138, 1922–1931. (c) Shearer, J.; Vasiliauskas, D.; Lancaster, K. M. Bonding and the role of electrostatics in driving C-C bond formation in high valent organocopper compounds. *Chem. Commun.* **2022**, *59*, 98–101. (d) Carsch, K. M.; DiMucci, I. M.; Iovan, D. A.; Li, A.; Zheng, S. L.; Titus, C. J.; Lee, S. J.; Irwin, K. D.; Nordlund, D.; Lancaster, K. M.; Betley, T. A. Synthesis of a copper-supported triplet nitrene complex pertinent to copper-catalyzed amination. *Science* **2019**, 365, 1138–1143.
- (46) (a) DiMucci, I. M.; Titus, C. J.; Nordlund, D. N.; Bour, J. R.; Chong, E.; Grigas, D. P.; Hu, C.-H.; Kosobokov, M. D.; Martin, C. D.; Mirica, L. M.; Nebra, N.; Vicic, D. A.; Yorks, L. L.; Yruegas, S.; MacMillan, S. N.; Shearer, J.; Lancaster, K. M. Scrutinizing Formally Ni<sup>IV</sup> Centers through the Lenses of Core Spectroscopy, Molecular Orbital Theory, and Valence Bond Theory. *Chem. Sci.* **2023**, *14*, 6915–6929. (b) Shreiber, S. T.; DiMucci, I. M.; Khrizanforov, M. N.; Titus, C. J.; Nordlund, D.; Dudkina, Y.; Cramer, R. E.; Budnikova, Y.; Lancaster, K. M.; Vicic, D. A. [(MeCN)Ni(CF<sub>3</sub>)<sub>3</sub>]<sup>-</sup> and [Ni(CF<sub>3</sub>)<sub>4</sub>]<sup>2</sup>: Foundations toward the Development of Trifluoromethylations at Unsupported Nickel. *Inorg. Chem.* **2020**, *59*, 9143–9151.
- (47) Desnoyer, A. N.; He, W.; Behyan, S.; Chiu, W.; Love, J. A.; Kennepohl, P. The Importance of Ligand-Induced Backdonation in the Stabilization of Square Planar d<sup>10</sup> Nickel  $\pi$ -Complexes. *Chem.—Eur. J.* **2019**, 25, 5259–5268.
- (48) Mena, M. R.; Kim, J.-H.; So, S.; Ben-Daat, H.; Porter, T. M.; Ghosh, C.; Sharma, A.; Flores, M.; Groy, T. L.; Baik, M.-H.; Trovitch, R. J. Comparing the Electronic Structure of Iron, Cobalt and Nickel Compounds That Feature a Phosphine-Substituted Bis(imino)pyridine Chelate. *Inorg. Chem.* **2022**, *61*, 6438–6450.
- (49) Koch, D.; Manzhos, S. The role of solvent charge donation in the stabilization of metal ions in aqueous solution. *MRS Commun.* **2018**, *8*, 1139–1144.

- (50) Gilson, R.; Durrant, M. C. Estimation of the  $pK_a$  values of water ligands in transition metal complexes using density functional theory with polarized continuum model solvent corrections. *Dalton Trans.* **2009**, 10223–10230.
- (51) Galstyan, G.; Knapp, E.-W. Computing  $pK_a$  Values of Hexa-Aqua Transition Metal Complexes. *J. Comput. Chem.* **2015**, *36*, 69–78.
- (52) Jackson, V. E.; Felmy, A. R.; Dixon, D. A. Prediction of the pK<sub>a</sub>'s of Aqueous Metal Ion +2 Complexes. *J. Phys. Chem. A* **2015**, *119*, 2926–2939.
- (53) Agarwal, R. G.; Coste, S. C.; Groff, B. D.; Heuer, A. M.; Noh, H.; Parada, G. A.; Wise, C. F.; Nichols, E. M.; Warren, J. J.; Mayer, J. M. Free Energies of Proton-Coupled Electron Transfer Reagents and Their Applications. *Chem. Rev.* **2022**, *122*, 1–49.
- (54) Mayer, J. M. Understanding Hydrogen Atom Transfer: From Bond Strengths to Marcus Theory. *Acc. Chem. Res.* **2011**, *44*, 36–46.
- (55) Tomás, R. A. F.; Bordado, J. C. M.; Gomes, J. F. P. *p*-Xylene Oxidation to Terephthalic Acid: A Literature Review Oriented toward Process Optimization and Development. *Chem. Rev.* **2013**, *113*, 7421–7469.
- (56) Denisov, I. G.; Makris, T. M.; Sligar, S. G.; Schlichting, I. Structure and Chemistry of Cytochrome P-450. *Chem. Rev.* **2005**, *105*, 2253–2277.